Colloid Polym Sci 277:762–776 (1999)

ORIGINAL CONTRIBUTION

A. Hieke
H.-D. Dörfler

Methodical developments for X-ray diffraction measurements and data analysis on lyotropic liquid crystals applied to K-soap/glycerol systems

Received: 3 March 1999
Accepted in revised form: 29 March 1999

Abstract X-ray diffraction (XRD) data acquisition and processing software measurements on long-spacing binary systems, including adapted noise reduction algorithms, has been developed. The computation of XRD patterns has been summarized and the origin of the distinct patterns of long-spacing compounds has been illustrated with the aid of such simulations. This also provided the possibility to evaluate the retrievable amount of information used for graphical or numerical indexing programs. Numerical indexing programs were applied and limits of indexing method have been discussed. Differential scanning calorimetry (DSC) measurements and temperature-dependent XRD measurements have been carried out for the concentrations $x_{KC_{12}} = 0.50$ and 0.30 of the K-laurate/glycerol system. The analysis of the small- and wide-angle diffractograms in the various phase regions of the binary system as well as the DSC measurements provided the following results:

- The creation of the lamellar phase extends over a temperature range of $\Delta T \approx 20$ K at a concentration of $x_{KC_{12}} = 0.50$. The lamellas show a reduced degree of order.
- The crystalline-to-gel phase transition is accompanied by a leap in the d values corresponding to the small-angle reflexes. Also a distinct splitting of the small-angle reflexes is observed within the gel phase. Simultaneously a rearrangement and intensity decay of the wide-angle reflexes occurs. Since some wide-angle reflexes are still present, the structure can be considered to have a partially reduced three-dimensional order.
- During the creation of lamellar phases the d value decreases sharply with rising temperature. This decrease of d can be interpreted as a further decay of molecular order in the hydrocarbon chains of the K-laurate within the bilayers.
- The XRD measurements correlate with the DSC data. According to our measurements a revision of the phase diagram with respect to the actual extension of the gel-phase region was necessary.

Key words X-ray diffraction · Data acquisition · Indexing · Lyotropic liquid crystals · K-laurate

Dedicated to Professor Dr. Dr. h. c. G. Lagaly on occasion of his 60th Birthday

A. Hieke · H.-D. Dörfler (✉)
TU Dresden, Institut für Physikalische Chemie und Elektrochemie
Kolloidchemie, Mommsenstrasse 13
D-01062 Dresden, Germany

Introduction

It is well known that lyotropic mesophases are mainly formed in multicomponent systems where solvent supports the formation of mesophases of amphiphilic compounds by favoring a suitable structure. In particular, a great number of binary systems of the type surfactant/water and ternary and quaternary systems

have been systematically studied in the last 50 years. In all the binary systems water has been used as a solvent.

Of course, the question arises of what influence other types of solvent, for instance, protic and aprotic liquids, will exert on the formation of lyotropic mesophases. In the literature, we find only the very first attempts to obtain some information about nonaqueous liquid crystals. The important papers in this area have already been summarized [1].

Our previous investigations with polarized microscopy texture observations [1] discussed five binary phase diagrams of K-soap/glycerol in order to study the influence of glycerol on the formation of lyotropic mesophases and gel (G) phases compared to water as a solvent. Independent of the chain length of the K-soaps (KC_{12}, KC_{14}, KC_{16}, KC_{18}, KC_{22}) all binary systems formed the same phase types. Besides lamellar (L_α) and hexagonal (H_α) phases, G and crystalline (C) phases were observed. Differences between the phase diagrams are basically found in the chain-length dependence and the actual temperature/concentration ranges of the phases. Further diversification had been observed in the K-myristinate/glycerol (KC_{14}/Gl) and K-stearate/glycerol (KC_{18}/Gl) systems, which showed an additional isotropic phase (I) and probably two G phases G_1 and G_2 according to the polarized microscopy observations. The object of our further investigations was to reveal the true nature of these regions as subsequently discussed.

The following generalizations about the existence of the phases in the binary phase diagrams can be made on the basis of polarized microscopy texture observations.

- The majority of the observed phase transitions occur at low temperatures out of a C phase.
- Above a certain minimum concentration of K-soap, micelles build up (isotropic S phase) followed by H phases.
- Following the H phases, the binary systems form L_α phases for high soap concentrations.

The order of appearance of the phase regions was found to be reproducible for all systems. However, the polarized microscopy investigations revealed that it is possible to undercool phase transitions significantly.

The knowledge of the existence of the different phase regions in the binary systems [1] established the basis for the following structural X-ray diffraction (XRD) investigations and differential scanning calorimetry (DSC) measurements. To ensure that the XRD measurements were carried out on identical phases, the same samples were used for the DSC measurements as well as additional polarized microscopy texture observations. The XRD studies on the five K-soap/glycerol systems, discussed in the following paper, were to answer primarily these questions.

- To which degree do the phase regions found by polarized microscopy correspond with the results from XRD and DSC?
- Are there further structural changes with the single-phase regions?
- What structures form the so-called G_1, G_2 and I phases? Are these really independent single phases?

The results of our investigations will be discussed for each system K-laurate/glycerol (KC_{12}/Gl), K-myristinate/glycerol (KC_{14}/Gl), K-palmitate/glycerol (KC_{16}/Gl), K-stearate/glycerol (KC_{18}/Gl), and K-behenate/glycerol (KC_{22}/Gl) in the following paper.

Methods

XRD measurements

The XRD measurements were carried out with the HZG4 horizontal counter diffractometer manufactured by the former Freiberger Präzisionsmechanik, Freiberg/Saxony, Germany (now Seifert FPM, Germany). Due to the weak diffraction signals caused by the organic and poorly ordered structures the optical setup required special attention and a delicate balance between resolution and signal intensity to optimize the measurement time. Samples were contained in rotating capillaries with 10-μm thick walls subject to transmission diffraction. Primary and secondary vertical so-called soller collimators, slits as well as special adjustable precision mechanical horizontal apertures (adjustable in steps of $\Delta x = \pm 2\,\mu$m) for suppressing scattered radiation were used. Provided correct adjustment, only about $r = 65$–$90\,\mu$m of the cylindrical sample core was exposed to radiation and small minimum starting angles of $2\Theta_{min} \approx 1^\circ$ equivalent to $d \approx 8.8$ nm for CuK_α radiation were achieved. Furthermore, a secondary graphite monochromator was used. Sample temperature stabilization with a deviation of $|\Delta T| = 0.1$ K was realized with a digitally controlled high-precision thermostat developed by us [1–3].

Polarized microscopy texture observations

To ensure correlation with the XRD measurements and for additional qualitative structural information, the samples were also checked by polarized microscopy [1]. A Jenapole 30-0060 stereoscopic microscope (Carl Zeiss Jena, Germany) equipped with an FP82 microsample thermostat adapter and with an FP80 control unit (both Mettler, Germany) were used. Effective texture identification of the lyotropic mesophases was supported by image recording during temperature ramping utilizing S-VHS video equipment (camera WV CL 700/G, recorder NV-FS88EG and monitor BT-H1450Y, all Panasonic, Japan). Optionally the Screen Machine video frame grabber (Fast Electronics, Germany) was used to provide digital representation of images for further computational enhancements.

Calorimetric measurements

The calorimetric measurements had supporting character, mainly to verify and confirm the polarized microscopy texture observations and XRD measurements. A type 121 calorimeter (Setaram, France) with an operational range of $T = 153$–1130 K, temperature ramp rates of $\Delta T/\Delta t = 0.0$ to ± 20.0 K/min, and a detection threshold of about $P_{min} \approx 10\,\mu$W was used. The special advantage of this type of calorimeter is its ability to employ hermetically sealed sample capsules preventing any evaporation of the solvent of

the mixture. The thermograms were used to determine the onset and offset temperatures of the phase transitions and were compared with the results from the polarized microscopy texture observations and XRD measurements. Especially the correlation with XRD data obtained from measurements at numerous rising temperature steps allowed confirmation of and insight into the observed structural phenomena.

Required software developments for the structural investigations

Acquisition and processing of the X-ray diffractometer data

Overcoming the limitations of the APX63 control software

The following statements apply specially to the software APX63 supplied with the HZG4 diffractometer from Seifert FPM; however, similar problems are likely to arise with comparable XRD equipment and therefore are of general interest. The APX63 data acquisition software, also used to control the diffractometer, had originally been designed to be used on powder diffractograms of well-ordered crystals providing distinct data patterns with intense and sharp reflexes. This resulted in some severe restriction with respect to the intended investigations. Diffractograms obtainable from lyotropic mesophases show significantly different characteristics and demand special data treatment. Consequently, the following restrictions needed to be overcome:

- The smallest value on the intensity axis was $I = 100$ cps, which was much too high. The zoom function into very small I and 2Θ ranges was unsatisfactory.
- Peak search and especially smoothing algorithms for noise reduction were only efficient on sharp peaks and were therefore unusable for our purposes.
- Range scanning in 2Θ has generally been possible in terms of goniometer control; however, without data accumulation, neither on-line nor off-line.
- Proprietary data formats were used and data exchange with other programs was not supported [4].

This led us to use APX63 only to control the goniometer and to launch the measurement jobs as well as to provide the initial unaccumulated data files. Therefore it was necessary to develop routines which could acquire on-line the files written by APX63 and provide all further data processing and display.

Data acquisition: APX file formats, on-line and off-line accumulation

The file format used by APX63 as disclosed in Ref. [4] uses ASCII code and consists of a 24-line header containing measurements information such as the 2Θ range, $\Delta 2\Theta$ steps, the time per step, etc., followed by the intensities. While simple and easily accessible for self-written code, these files are hard to read with any general-purpose data processing program.

It is often difficult to predetermine the time required for a certain XRD measurement. For example, if the existence of a peak at a certain position needs to be clearly established it is extremely helpful to have the possibility to sweep over a 2Θ range with repeated fast measurement until a satisfactory signal-to-noise ratio is obtained. Therefore, the files written by APX63 during these scans were constantly checked for changes by a program running parallel and, if required, the new impulse height data were instantly provided for on-line accumulation and display. The measurements could be terminated at any point in time; however, routine measurements were unattended and the files gathered were accumulated off-line [3].

Data noise reduction

As already mentioned, the lyotropic mesophases investigated provide only very low small- and intermediate-angle XRD signal intensity, typically of the order of some $I = 10$–100 cps. Therefore, one of the most important aspects of data processing is to apply efficient and adapted digital filters or general noise reduction algorithms.

Unfortunately, there is no principal difference between signal and noise usable for separation of the components. Through the diffractograms may have typical space frequency spectra this fact cannot be used for noise reduction.

Commonly used smoothing procedures for sharp peaks do not yield satisfactory results if applied to diffractograms from lyotropic mesophases containing wide superimposed peaks and bands.

Furthermore, in small- and intermediate-angle XRD one observes that for decreasing diffraction angles the 2Θ peaks become increasingly asymmetric due to convolution effects. Noise reduction on these peaks may cause remarkable peak position shift, generally in a direction towards lower angles. The resulting error for the corresponding d value rises rapidly with decreasing diffraction angle.

Different digital filters for use in the spatial and the frequency domain have been compared with respect to noise suppression and peak position preservation. A method was developed that adjusts the strength of a spatial domain filter according to the impulse height of the values to be smoothed. Thereby optimum noise reduction and peak position preservation was achieved while less computational effort was required compared to fast Fourier transform techniques.

Alternatively, the second well-known method for noise reduction, operating in the frequency domain, was

used in some cases utilizing an improved so-called DFT technique. The Blackman window, recommended by Chornik et al. [5] in connection with deconvolution, was chosen and was applied with satisfactory results to the diffractograms discussed.

Details can be found in Ref. [3], and the reader is also referred to Refs. [5–15] as well to as some of the application-oriented works [16–19].

Origin of the distinct XRD patterns of long-spacing compounds

Calculation of X-ray powder diffraction patterns

Subsequently the principal calculation of X-ray powder diffraction reflexes and their intensities shall briefly be outlined as it provides insight into the origin of the characteristic diffractograms of lyotropic mesophases, or more generally, of long-spacing compounds. Furthermore, it allows an understanding of the different approaches to indexing these diffractograms as well as reasons for the limited amount of information available.

As is well known (e.g., Ref. [20]), the distances $d(h,k,l,a,b,c,\alpha,\beta,\gamma)$ between crystallographic planes of a triclinic unit cell, determining the position of the XRD reflexes, may be calculated by

$$\frac{1}{d^2} = \frac{1}{V^2}(s_{11}h^2 + s_{22}k^2 + s_{33}l^2 + 2s_{12}hk + 2s_{23}kl + 2s_{13}hl) \quad (1)$$

with

$$V^2 = a^2b^2c^2(1 - \cos^2\alpha - \cos^2\beta - \cos^2\gamma + 2\cos\alpha\cos\beta\cos\gamma) \quad (2)$$

the volume of the unit cell

$$s_{11} = b^2c^2\sin^2\alpha \quad (3)$$

$$s_{22} = a^2c^2\sin^2\beta \quad (4)$$

$$s_{33} = a^2b^2\sin^2\gamma \quad (5)$$

$$s_{12} = abc^2(\cos\alpha\cos\beta - \cos\gamma) \quad (6)$$

$$s_{23} = a^2bc(\cos\beta\cos\gamma - \cos\alpha) \quad (7)$$

$$s_{13} = ab^2c(\cos\gamma\cos\alpha - \cos\beta) \quad (8)$$

the reciprocal unit cell parameters multiplied by V^2 and by $h,k,$ and l, the Miller indices, and $a,b,c,\alpha,\beta,$ and, γ the unit cell parameters.

According to

$$I \cong H\,P\,L|F|^2 \quad (9)$$

the relative intensity of reflexes from powder diffractograms of perfect crystals are mainly proportional to

– The multiplicity factor $H(h,k,l)$.

– The polarization factor.

$$P = \frac{1 + \cos^2(2\Theta)\cos^2(2\Theta_{MC})}{1 + \cos^2(2\Theta_{MC})} \quad , \quad (10)$$

where $2\Theta_{MC}$ is reflection angle of the monochromator.

– The Lorenz factor

$$L = \frac{1}{\sin^2\Theta\cos\Theta} \quad . \quad (11)$$

– The structure factor F.

The structure factor [21] takes into account the arrangement of atoms within nonprimitive unit cells, superimposing the waves scattered by each single atom, and is expressed by

$$F = \sum_{i=1}^{na} {}^a f_i \exp[2\pi j(hx_i + ky_i + lz_i)] \quad , \quad (12)$$

where x_i, y_i, z_i is the relative position of the ith atom within the unit cell with respect to the edges $a, b,$ and c, and ${}^a f_i$ are the atomic scattering factors of the ith atom.

The coefficients used to calculate approximations of the atomic scattering factors according to

$${}^a f_i = \sum_{m}^{4} {}^a a_m \exp\left[-{}^a b_m \frac{\sin^2\Theta}{\lambda^2}\right] + {}^a c + {}^a\delta f' + {}^a\delta f'' \quad (13)$$

with ${}^a a_m, {}^a b_m, {}^a c$ as element specific coefficients, ${}^a\delta f', {}^a\delta f''$ as coefficients for the correction of dispersion, and Θ the (half) diffraction angle may be taken from Refs. [22, 23].

The formulas described above have been implemented in code to predict powder diffraction patterns. As shown later, this is closely related to the inverse problem: the determination of the unit cell parameters from a given diffractogram.

Indexing of X-ray powder diffraction patterns with special respect to long-spacing crystals

Since the 2Θ position of the XRD reflexes is only determined by the unit cell parameters a,b,c,α,β and γ the problem of indexing such powder diffraction patterns is equivalent to finding a point in six-dimensional space with the unit cell parameters as axes. The location of possibly several hundred or thousand atoms within the unit cell influences only the intensity of the reflexes, including the possibility of extinction.

Historically, graphical indexing methods were used first to determine unit cell parameters from powder diffraction patterns followed by pure numerical/computational methods. Nevertheless, all methods face the same problem of locating the six-dimensional vector.

Depending on the characteristics of the diffractograms measured, the information available may be insufficient to obtain this solution.

Especially for long-spacing crystals, three graphical methods proposed by Vand [24, 25] in 1948, and applied to potassium caproate, are known and have been used since. The principal idea [24] is to decompose the equation

$$\frac{1}{d_{hkl}^2} = D_{hkl}^{*2} = h^2a^{*2} + k^2b^{*2} + l^2c^{*2} + 2klb^*c^*\cos\alpha^* + 2lhc^*a^*\cos\beta^* + 2hka^*b^*\cos\gamma^* \quad (25)$$

containing the reciprocal unit cell parameters a^*, b^*, c^*, α^*, β^*, and γ^* (and equivalent to Eq. 1) into

$$D_{hkl}^{*2} = H_{hk}^{*2} + L_{hkl}^{*2} \quad (26)$$

with

$$H_{hk}^{*2} = h^2A^{*2} + k^2B^{*2} - 2hkA^*B^*\cos\gamma \quad (27)$$

$$L_{hkl}^{*2} = lc^* + hA^*\cot\beta^* + kB^*\cot\alpha^* \quad (28)$$

and

$$A^* = a^*\sin\beta^* \quad (29)$$

$$B^* = b^*\sin\alpha^* \quad (30)$$

Since c^* is small compared to a^* and b^* in the case of long-spacing crystals, the diffractograms consist of characteristic so-called bands, as explained in detail later. These bands are created by reflexes with constant h and k but variable l since L_{hkl}^* varies only slightly according to Eq. (28). Within a band D_{hkl}^* is mostly determined by H_{hkl}^*. This is equivalent to a decomposition of the crystal into two-dimensional and one-dimensional periodicity; therefore Eqs. (26)–(28) can be solved graphically.

However, this approach may only be successful for a single-compound system of high crystallographic perfection and provides no information about the remaining uncertainty of the solution found. The method faces severe problems if applied to the lyotropic mesophases investigated. This is mainly due to the fact that necessary reflexes with high h and k cannot be obtained since their intensity is too low. The main reasons are lattice imperfections, the composition of light elements, and the presence of a solvent. Secondly, even if these reflexes could be obtained, the remaining uncertainty in determining the head of band 25 jeopardizes the successful indexing.

Numerical indexing methods commonly use

$$\sin^2\Theta = \frac{\lambda^2}{4V^2}\left(s_{11}h^2 + s_{22}k^2 + s_{33}l^2 + 2s_{12}hk + 2s_{23}kl + 2s_{13}hl\right) \quad (31)$$

referred to as a quadratic formulation, and which is again equivalent to Eq. (1). Furthermore, the substitution

$$Q = \sin^2\Theta \quad (32)$$

is used. A set of angle Θ_i is taken from the reflexes of a diffractogram and the corresponding Q_i are calculated. A set of s_{11}, s_{22}, s_{33}, s_{12}, s_{23}, s_{13} (equivalent to a, b, c, α, β, γ) is searched for that satisfies

$$Q_i - \Delta Q_i < \frac{\lambda^2}{4V^2}\left(s_{11}h^2 + s_{22}k^2 + s_{33}l^2 + 2s_{12}hk + 2s_{23}kl + 2s_{13}hl\right) < Q_i + \Delta Q_i \ , \quad (33)$$

with ΔQ_i an arbitrary error threshold. The angles $2\Theta_i$ have to be provided with a precision of the order of $\Delta 2\Theta \approx 0.01$–$0.20°$, which is in general possible for nearly perfect crystals. However, Eq. (33) can be satisfied with different sets of s_{ij} since small s_{ij} may be compensated with higher h, l, k. Therefore, it is also required that the first reflexes have the smallest indices and the volume of the unit cell is a minimum.

Several indexing programs use Eq. (33), one of the first papers in the field by Werner [27] dates back to 1964. Among others [26], the program TREOR [28] has been used for numerous unsuccessful attempts to index measured diffractograms from crystalline phases of the lyotropic mesophases discussed. The likely reasons are given later.

As mentioned previously, relatively high demands on the precision of angular resolution and determination of the reflexes have to be applied, since all reflexes are registered in only one dimension. The lower the symmetry of a unit cell, the stronger the demands due to the increased diversity of reflexes as emphasized in Ref. [28]. The required errors (and resolutions) of $|\Delta 2\Theta| < 0.02°$ can usually be obtained from focusing optical setups, but not from transmission diffraction. Generally, about 20 reflexes have to be known with this precision for successful indexing attempts. Indexing with less precise data does not yield less precise results, but no results at all.

Such numbers of reflexes are barely obtainable from the diffractograms of the lyotropic mesophases, since all small-angle reflexes are only higher orders of the 001 reflexes and high reflex broadening prevents precise determination of the band heads. Depending on the chosen error threshold, ΔQ_i, programs provide either no or numerous solution. This means that insufficient information is at hand to narrow down the point searched for in the six-dimensional space of lattice parameters; however, this problem is not unique to TREOR or numerical methods but is of a general nature; each indexing algorithm, graphical or numerical method faces it. The reasons can be understood by

performing a numerical test of the origin of the diffraction patterns of long-spacing compounds with imperfect lattices as discussed in the next section.

Computation of X-ray powder diffraction patterns of long- spacing compounds

The atomic coordinates of molecules used for structure factor calculation in nonprimitive unit cells have been obtained from molecular modeling programs and read into our own code [3]. In addition to the utilization of Eqs. (1)–(13) the broadening of reflexes due to the necessary optics as well as lattice imperfection and potentially reduced coherently diffracting domains were taken into account for the simulations by using a convoluting function as explained in detail in Ref. [3]. Therefore, even by using equations derived for perfect crystals, the desired explanation of the observed characteristic diffractograms and the limited possibilities of indexing them could be given. Furthermore it is assumed that the solvent has no crystallographic order and provides only an amorphous background to the diffraction signal. This background signal can be found in measurements as a characteristically wide elevation, typically between $2\Theta \approx 15$–30° for CuK_α radiation.

Initially, primitive unit cells, containing only one atom, and no reflex broadening are assumed. Figure 1 shows from top to bottom

- A cubic unit with $a = 0.50$ nm. Due to the high symmetry, only six reflexes appear in the 2Θ range considered. The intensities of all reflexes are of the same order.
- A triclinic unit cell with $a = 0.45$ nm, $b = 0.50$ nm, $c = 0.55$ nm, $\alpha = 70^\circ$, $\beta = 80^\circ$, and $\gamma = 80^\circ$. The edges have been changed only slightly ($\leq 10\%$) but in combination with the asymmetry 37 reflexes emerge. The intensity range of the reflexes already exceeds 1 order of magnitude.
- A triclinic unit cell with $a = 0.45$ nm, $b = 0.50$ nm, $c = 1.0$ nm, $\alpha = 70^\circ$, $\beta = 80^\circ$, and $\gamma = 80^\circ$.
- A triclinic unit cell with $a = 0.45$ nm, $b = 0.50$ nm, $c = 2.0$ nm, $\alpha = 70^\circ$, $\beta = 80^\circ$, and $\gamma = 80^\circ$.
- A triclinic unit cell with $a = 0.45$ nm, $b = 0.50$ nm, $c = 4.0$ nm, $\alpha = 70^\circ$, $\beta = 80^\circ$, and $\gamma = 80^\circ$. 159 reflexes; intensity with 4 orders of magnitude.

As expected, the longer c becomes, the more the reflexes extend towards smaller angles. It is not obvious, however, that in the last example the intensity range of the 159 reflexes covers almost 4 orders of magnitude. One has to realize that the first and most intense reflex, which is considered to be 100% in these examples, in reality has an intensity of the order of 200–400 cps in the best cases. Due to the high number of reflexes the typical distance between the reflexes in the intermediate- and wide-angle range is $(2\Theta_{i+I} - 2\Theta_i) < 0.1^\circ$.

A simulated diffraction pattern for a triclinic unit cell with $a = 0.45$ nm, $b = 0.50$ nm, $c = 4.0$ nm, $\alpha = 70^\circ$, $\beta = 80^\circ$, and $\gamma = 90^\circ$ with broadening of reflexes taken into account is shown in Fig. 2. Since the reflexes are so narrow, the characteristic bands are created from known measurements. While the determination of reflexes for small angle $2\Theta < 10^\circ$ is not influenced, intermediate- and wide-angle reflexes are hard to resolve, even though the assumed reflex broadening is smaller than in reality. This is partially caused by an optical effect increasing the visible size of the diffracting sample core. At the bottom of Fig. 2 the range $2\Theta = 16$–22° is enlarged. For example, the 015 and the 010 reflexes superimpose. If the resulting peak were considered to be a 010 reflex, as would most likely be done in the measured diffractogram, the resulting error is $\Delta 2\Theta = -0.036^\circ$.

Even more severe in the problem for the 01-1, 101, 102, and 100 reflexes, which are impossible to resolve. If the maximum is ascribed to the 100 reflex, the error caused is $\Delta 2\Theta = -0.11^\circ$. These errors are the reason why the correct indexing of the diffraction patterns of the presumably triclinic unit cells in crystalline phases of the lyotropic mesophases investigated fails. It is not impossible to obtain an indexing solution by graphical or numerical methods, but it is most likely not be the correct one since only data with the errors mentioned can be given.

Again, the reflex broadening is basically caused by the nonfocusing transmission diffraction optics, lattice imperfection (including solvent), and possibly reduced coherently diffracting domains.

Further computer simulations revealed that the information is limited in that a^*, b^*, c^*, and γ^* can be determined, while α^* and β^* are inaccessible. The search for the desired point can only be narrowed down to a two-dimensional hyperplane. It was found that four areas within this plane, positioned symmetrically with respect to the coordinate origin, are most likely to contain the true, yet unobtainable solution.

Finally, the computed results for the nonprimitive unit cell are given. Figure 3 shows from top to bottom

- A long-spacing tetragonal primitive unit cell (carbon).
- A long-spacing tetragonal nonprimitive unit cell with two K-stearate molecules.
- A long-spacing triclinic primitive unit cell (carbon).
- A long-spacing triclinic nonprimitive unit cell with two K-stearate molecules.

As expected, the tetragonal cells generate fewer separate reflexes than the triclinic cells. The 101 and 011 reflexes as well as the 111 and 1-11 reflexes superimpose in the tetragonal case and therefore yield higher relative intensity. This is not observed in measured diffractograms and therefore is further indication of the presence of triclinic cells in crystalline phases.

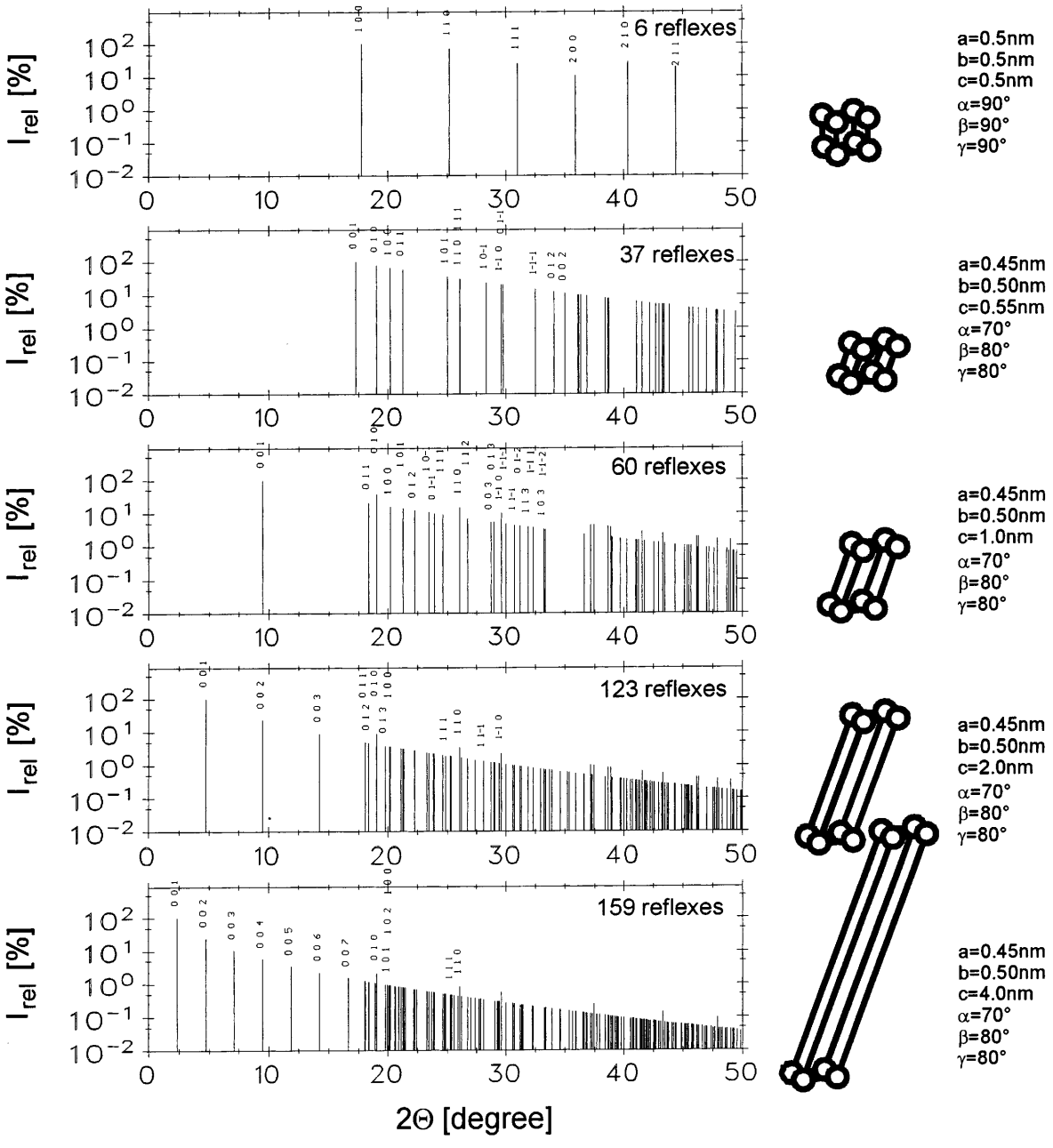

Fig. 1 Computed X-ray powder diffractograms – reflex position and relative intensity – showing the origin of the distinct X-ray diffraction (*XRD*) patterns in a series of diffractograms from a small-spacing cubic unit cell (*top*) to a long-spacing triclinic unit cell (*bottom*); primitive unit cells with 1 atom carbon and CuK_α radiation are assumed

However, the most remarkable effect is that due to the presence of molecules in the unit cell the structure factor is modified such that the relative intensity of the band heads is amplified (higher orders of 1 are attenuated). This would allow more precise determination of peak positions and might be the reason for successful graphical or numerical indexing attempts on diffractograms from pure metal–soap crystals. Vand's theory could not give information about the expected intensity of the reflexes.

Unfortunately, this advantageous effect is not observed in XRD measurements of the lyotropic mesophases investigated. The reasons are the partially melted and imperfectly aligned chains of the K-soaps in the lyotropic mesophases even at room temperature preventing this modification of the structure factor; therefore the bands remain broad and cannot be resolved.

Elevated temperature and high solvent concentration cause increased decay of the order in the chains and the

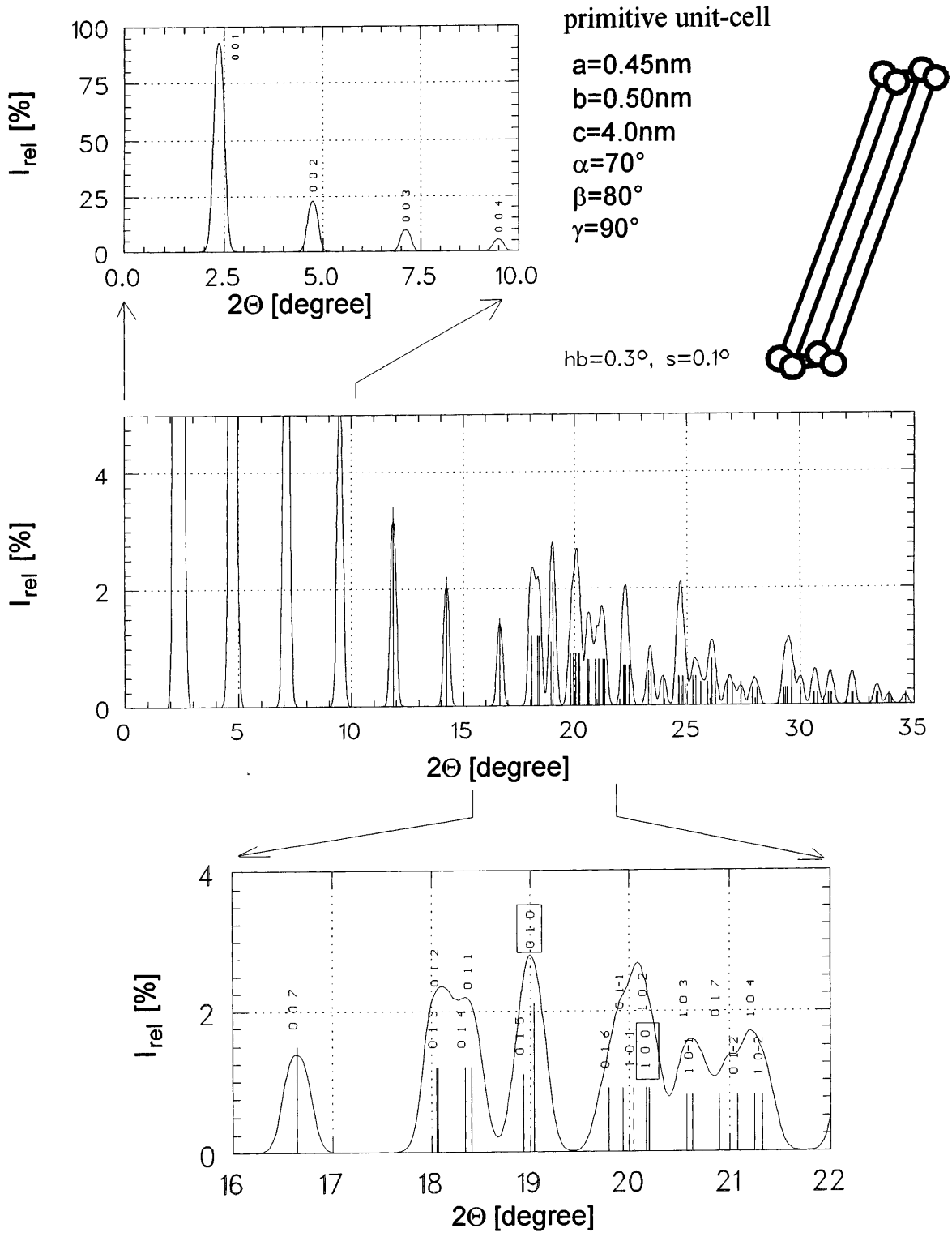

Fig. 2 Computed X-ray powder diffractogram for a long- spacing triclinic unit cell from carbon taking into account the reflex broadening due to imperfect crystallographic structure, solvent, and optical limitations by means of an additional convolution. *Top*: Enlarged small-angle range; 001 reflex scaled to 100% reflex intensity. *Middle*: complete simulated 2Θ range – no amorphous background added. *Bottom*: Enlarged range $2\Theta = 16$–$22°$. Several very narrow reflexes superimpose and create the characteristic bands making it practically impossible to determine the correct band head position

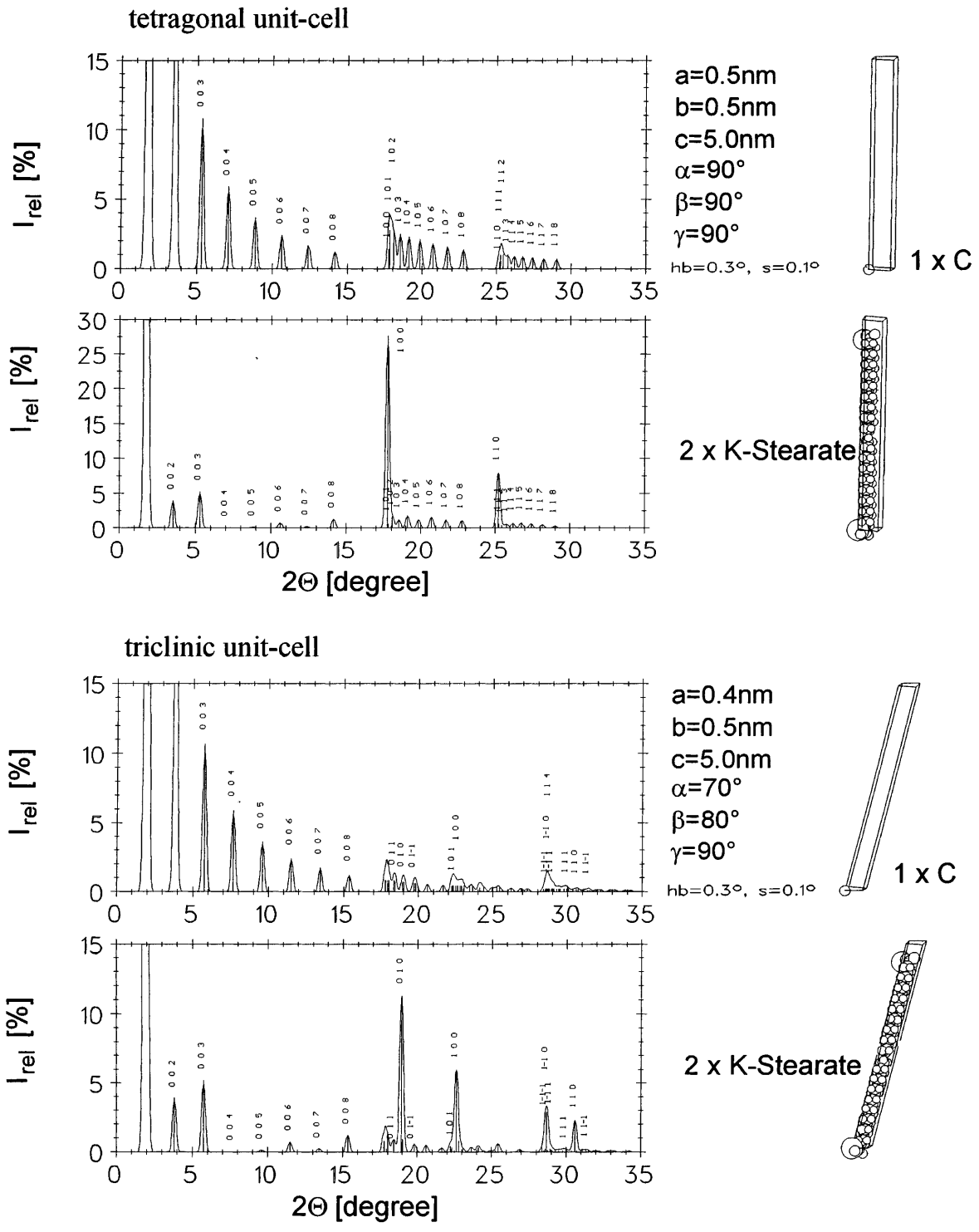

Fig. 3 Computed X-ray powder diffractograms for long-spacing tetragonal and triclinic primitive unit cells from carbon as well as for non primitive unit cells containing 2K-stearate molecules. Reflex broadening due to imperfect crystallographic structure, solvent, and optical limitations is taken into account by means of an additional convolution. Amplification of the relative intensity of the band heads in non primitive cells. Only valid for nearly perfect crystals and not observable in the crystallographically imperfect, lyotropic mesophases investigated

[a, b] plane and therefore further broadening of the bands and diminishing of the reflexes in angular ranges above $2\Theta \approx 10°$. Ultimately, L_α (and of course S) phases shown no crystallographic short-range order ("two-dimensional liquid") and consequently show total extinction of wide-angle XRD reflexes.

Selected investigation on the binary system K- laurate/glycerol (KG_{12}/Gl) as a function of temperature

Concentration $x_{KC_{12}} = 0.50$

The phase diagram of this binary system, obtained from polarized microscopy texture observations, is shown in Fig. 4a. Details have been discussed in Ref. [1]. From this system two samples at concentration $x_{KC_{12}} = 0.50$, 0.30 were investigated. According to the polarized microscopy observations the polymorphous transitions $C \leftrightarrow G \leftrightarrow L_\alpha$ are expected at the concentrations $x_{KC_{12}} = 0.50$ (see Fig. 4). Of special interest were the structural data of the L_α and G phases. At the temperature section $x_{KC_{12}} = 0.30$ the polymorphous transitions $C \leftrightarrow G \leftrightarrow H_\alpha \leftrightarrow S$ appear. Here, the structural data of the G and H_α phases were of interest.

Wide- and small-angle X-ray diffractograms as well as the DSC curves of this system with increasing temperature are shown in Figs. 5 and 6, respectively. A rearrangement and intensity decay of the wide-angle reflexes is observed. The typical splitting of the small-angle reflexes in only partially developed in this system and does not appear to be synchronous with the G phase. Not until $T = 363$ K are the split reflexes distinguishable on the right slope of the first reflex according to Fig. 6. Before this temperature only a reflex broadening is observable. This means, that the creation of the G phase is a temperature-dependent process.

Starting at $T = 398$ K, and in accordance with the onset temperature from the DSC curve, the creation of the L_α phase begins. As expected, with decreasing order in the plane of the lamellas the wide-angle XRD reflexes gradually disappear as can be seen in Fig. 5. At $T = 423$ K the L_α phase is completely established. The creation of the L_α phase spans a temperature range of $\Delta T \approx 20$ K. Within this range polarized microscopy observations show increasingly sharper images with rising temperature.

In the top portion of Fig. 7 the equivalent d values of the first small-angle reflexes and the DSC curves for heating and cooling are drawn for better quantitative comparability. In the bottom part of the figure the diffractogram for $T = 323$ and 363 K are displayed. One recognizes the split small-angle reflexes and the intensity-modified wide-angle reflexes of the G phase. Comparison of the curve also reveals the decreasing degree of spatial order. Since some weaker wide-angle range reflexes are still present in the G phase, the structure can be considered to have a reduced three-dimensional

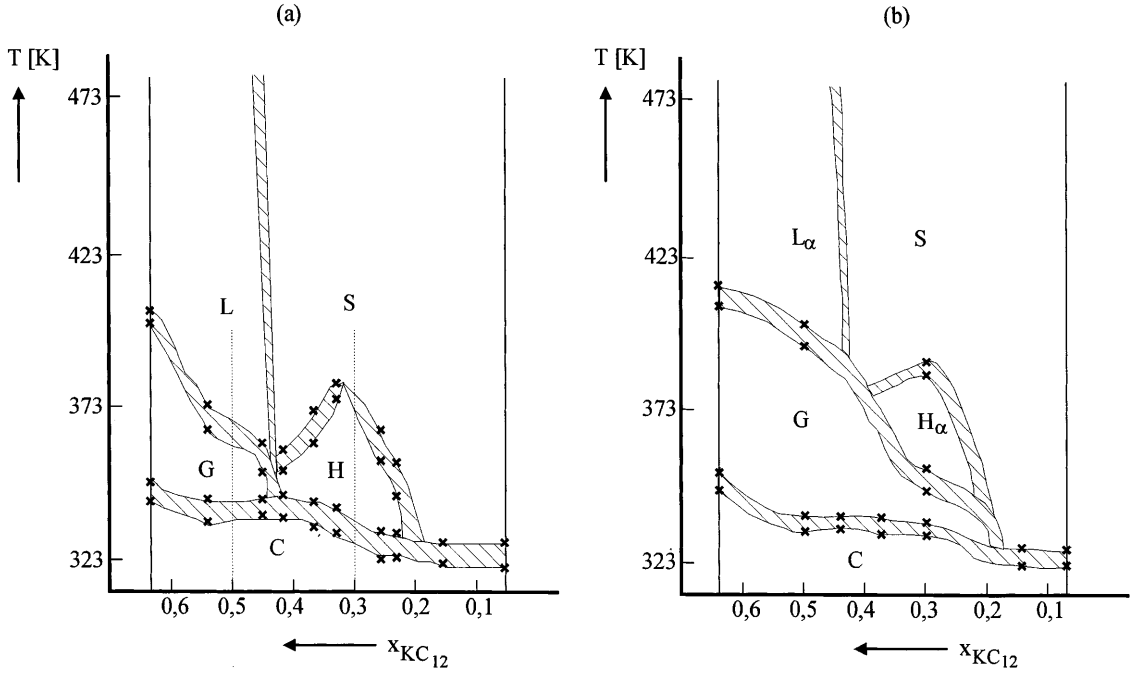

Fig. 4a, b Cutout of the phase diagram of the binary system K-laurate/glycerol (KC_{12}/Gl). **a** Phase diagram based on polarized microscopy texture observations according to Ref. [1]. **b** Revised phase diagram according to our XRD and differential scanning calorimetry (DSC) measurements, C = crystalline phase, G = gel phase, H_α = hexagonal phase, L_α = lamellar phase, S = isotropic micellar solution

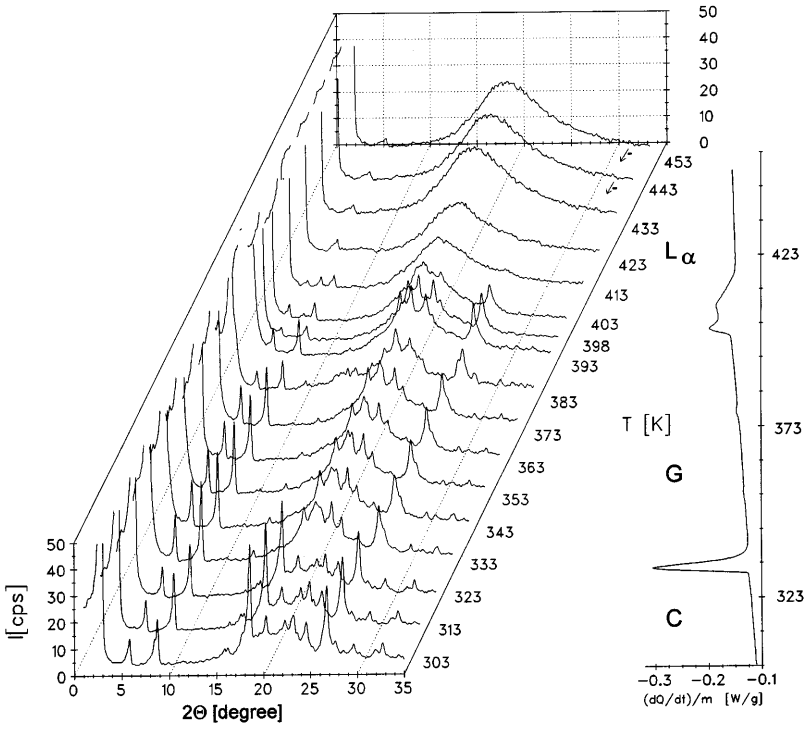

Fig. 5 Comparison of wide-angle X-ray diffractograms with the DSC curve for rising temperature for the KC_{12}/Gl system, concentration $x_{KC_{12}} = 0.50$

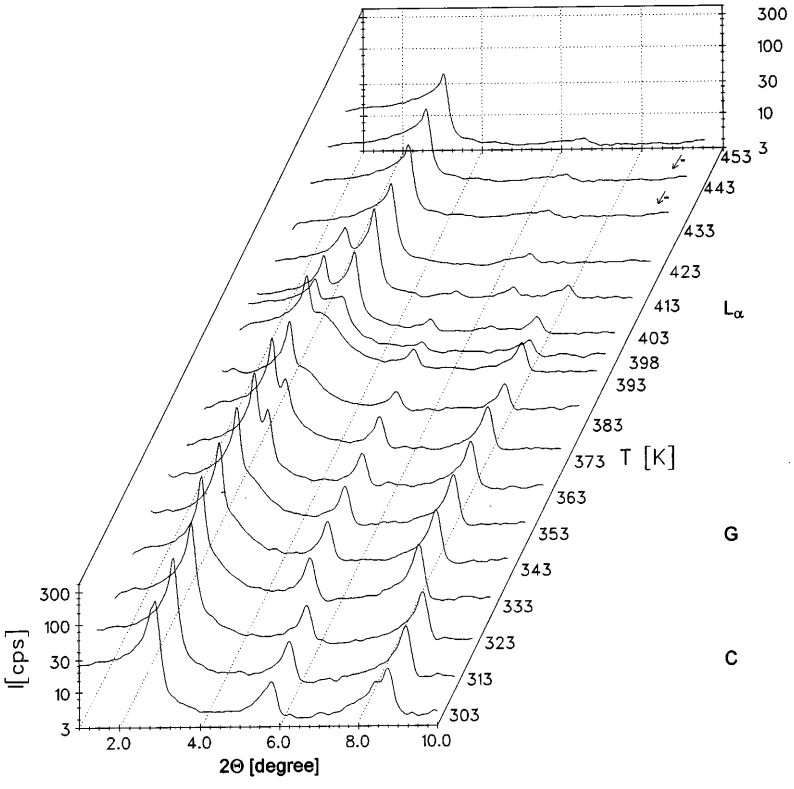

Fig. 6 Small-angle X-ray diffractograms for rising temperature for the KC_{12}/Gl system, $x_{KC_{12}} = 0.50$

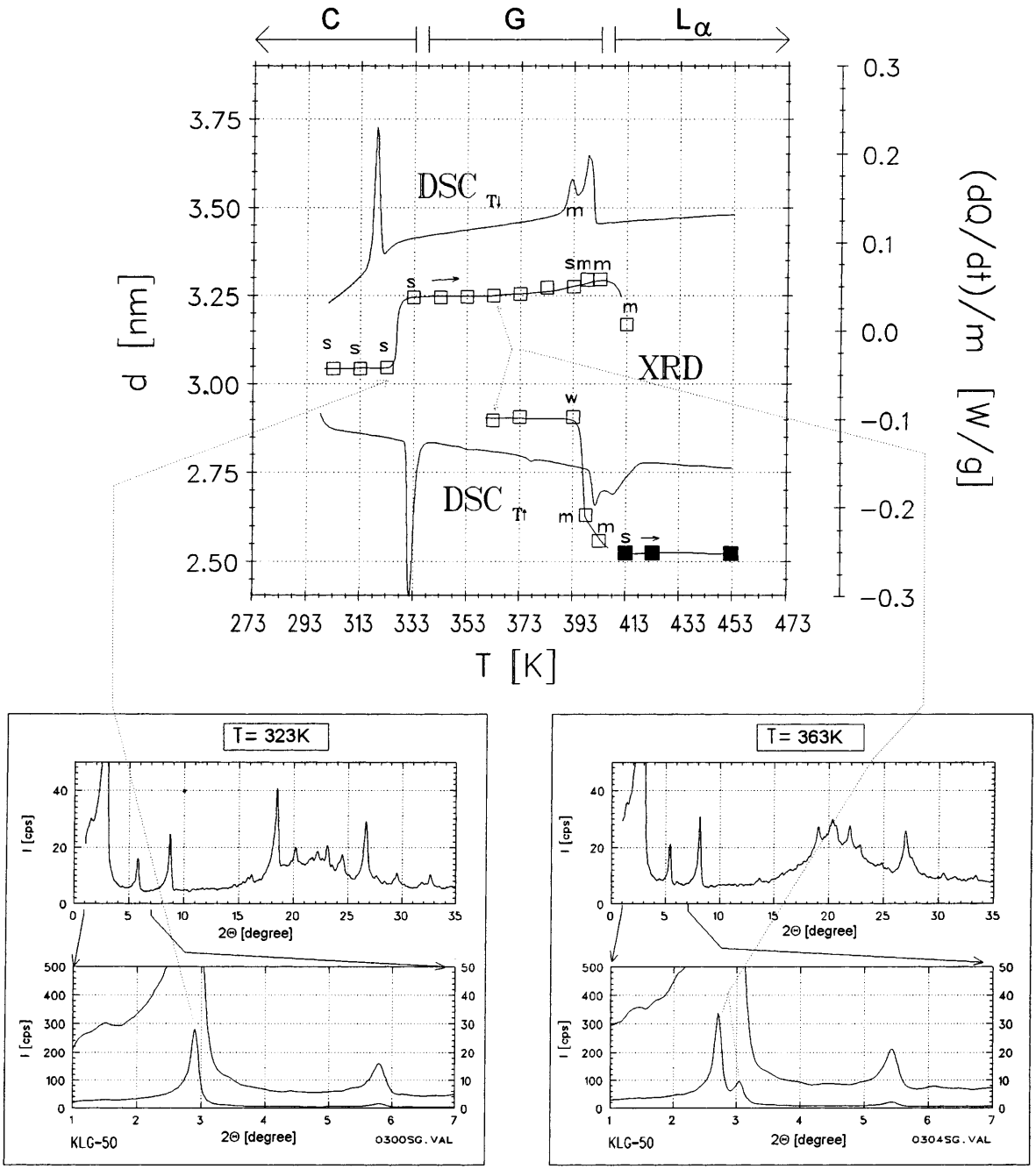

Fig. 7 *Top*: Comparison the d values of the first small-angle reflexes with the DSC curve obtained for rising and falling temperatures for the KC_{12}/Gl system, concentration: $x_{KC_{12}} = 0.50$. □ reflexes of the C and G phases, ■ reflexes of the L_α phase. Reflex intensity: w = weak, m = medium, s = strong *Bottom*: X-ray diffractograms for $T = 323$–363 K representing a C and a G phase; small-angle range enlarged. The association of the small-angle reflexes with d values in the *top portion* of the figure has been marked

order. The transition to the G phase is accompanied by a sharp shift of the small-angle 001 reflex equivalent to a leap in d of about $\Delta d \approx 0.21$ nm.

In contrast during the formation of the L_α phase in the temperature range $T = 393$–403 K the d value decreases rapidly as the distance of the lamellas is reduced. For further increases of temperature d stays constant within the temperature range considered. The decrease in d during the transition can be interpreted as a decay of molecular order in the hydrocarbon chains of the K-laurate. Obviously, the order of the lamellas is not perfect since only one higher order of the 001 reflex can be measured. Furthermore one finds that the phase-

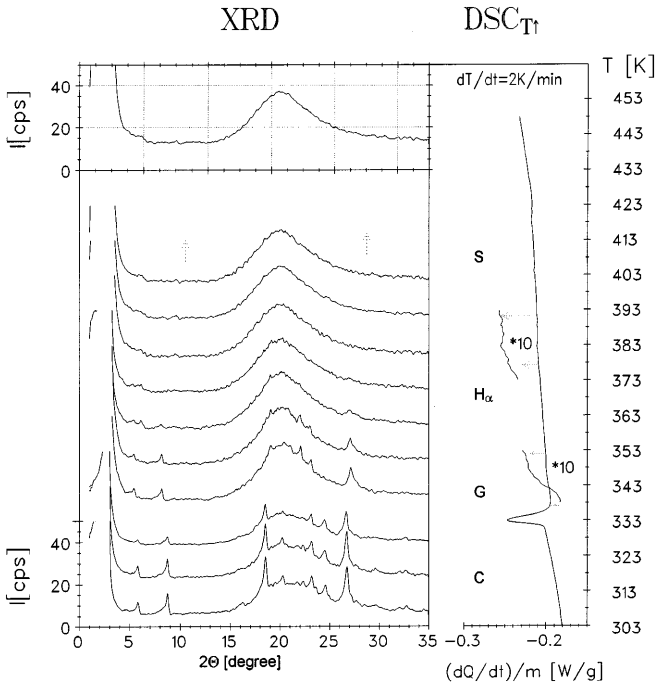

Fig. 8 Comparison of wide-angle X-ray diffractograms with the DSC curve for rising temperature for the KC_{12}/Gl system, $x_{KC_{12}} = 0.30$

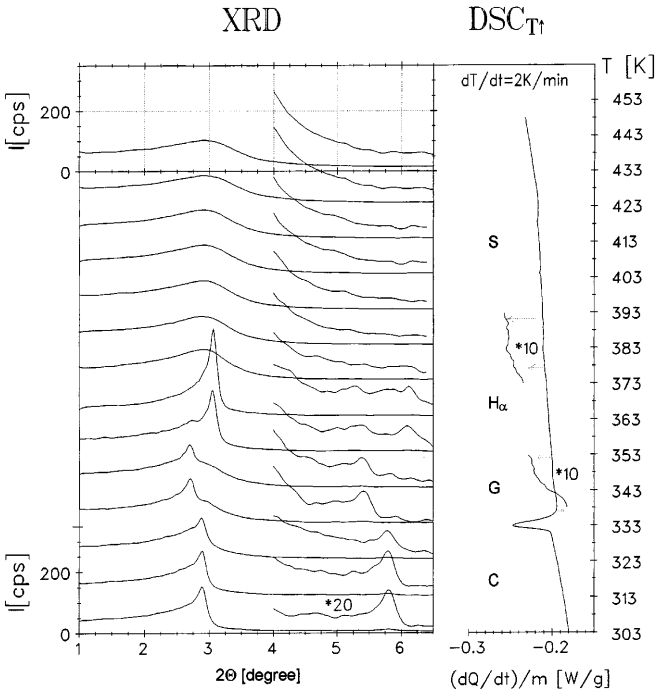

Fig. 9 Comparison of small-angle X-ray diffractograms with the DSC curve for rising temperature for the KC_{12}/Gl system, $x_{KC_{12}} = 0.30$

transition temperature interpolated from the XRD measurements fits exactly in middle of the phase-transition temperatures found from DSC curves obtained during heating and cooling.

Concentration $x_{KC_{12}} = 0.30$

The X-ray diffractograms as well as DSC curves of the system K-laurate/glycerol $x_{KC_{12}} = 0.30$ for the small- and wide-angle ranges are shown for rising temperatures in Figs. 8 and 9, respectively. Comparing the curves one finds that the G phase is created between the C phase and the H_α phase. The temperature range of the G phase is between $T = 333$ and 348 K. The diffractograms are similar to those of Figs. 5 and 6 and the distinct wide-angle reflexes of the G phase are again found as in Fig. 5.

Again, the transition from the C to the G phase is accompanied by a splitting of the small-angle reflexes; however this is perceptible as a shoulder in the small-angle reflex. This is best visible in Fig. 9 between $T = 333$ and 343 K. Within the H_α and S phases no short-range order exists and only the characteristic amorphous background is found in the wide-angle diffractograms.

In Fig. 10 the equivalent d values of the first small-angle reflexes and the DSC curves for heating and cooling are illustrated. Again, the transition to the G phase correlates to a sharp shift of the small-angle 001 reflex equivalent to $\Delta d \approx +0.20$ nm.

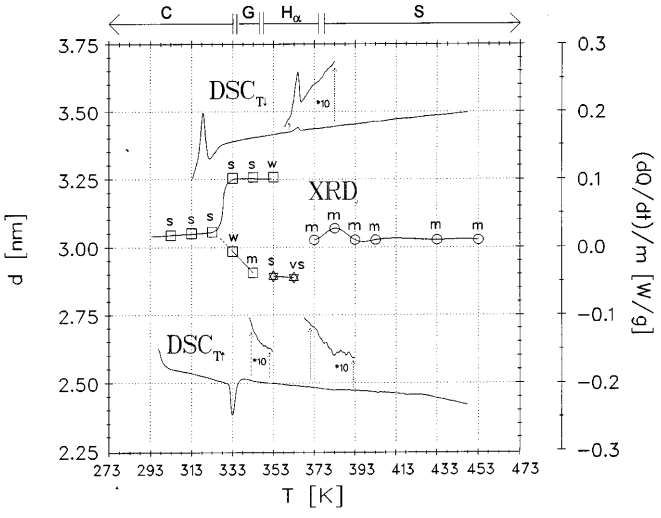

Fig. 10 Comparison the d values of the first small-angle reflexes with the DSC curve obtained for rising and falling temperatures for the KC_{12}/Gl system, $x_{KC_{12}} = 0.30$. □ reflexes of the C and G phases, ✡ reflexes of the H-phase, ○ reflexes of the isotropic solution. *vs* = very strong

The transition from the G phase to the H_α and S phases is thermally significantly weaker than the transition from the C to the G phase and is only visible in the DSC curves after much enlargement. These transitions are close to the detection threshold.

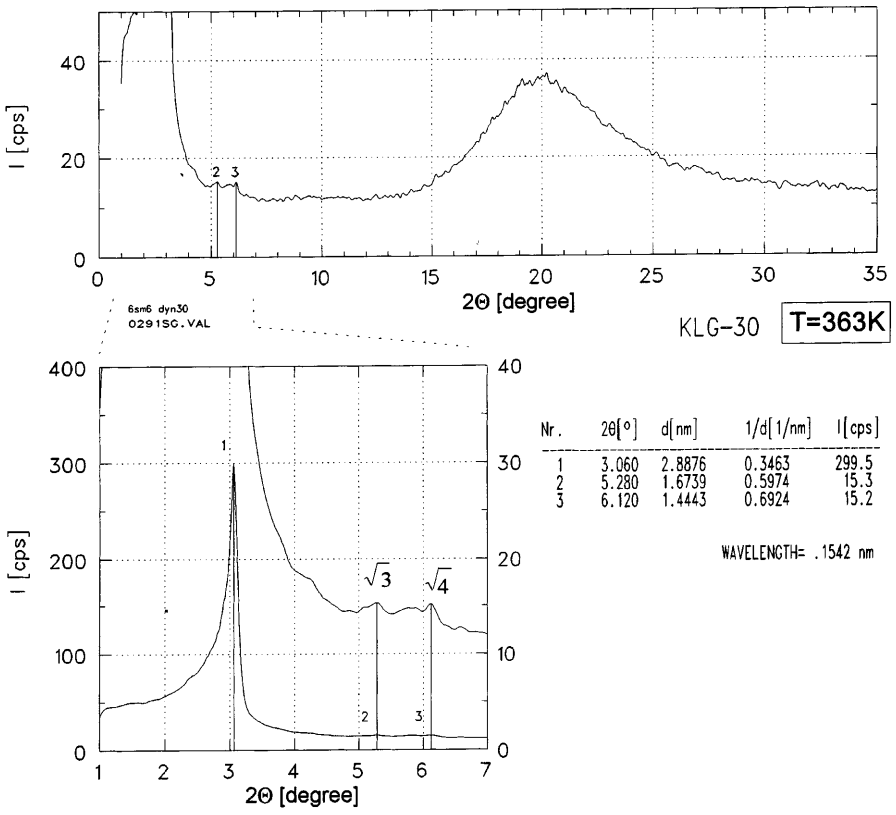

Fig. 11 Small- and wide-angle X-ray diffractograms for $T = 363\,\mathrm{K}$ within the hexagonal phase of the KC_{12}/Gl system, $x_{KC_{12}} = 0.30$

Remarkably, the phase transition G ↔ C does not appear in the DSC measurement within the range of detectability if the system is cooled down. The polarized microscopy texture observations could not confirm the existence of the G phase. Still, the region of the G phase extends below the L_α as well as the H_α phase to a concentration of approximately $x_{KC_{12}} \approx 0.26$.

According to Fig. 11, and as in all systems investigated, H_α phases generally yield a relatively intense and sharp first small-angle reflex, usually even sharper than the 001 reflex in C phases. However, the second reflex, which is crucial for the unequivocal identification of the H_α phase, is positioned according to a d value ratio of $1{:}\sqrt{3}$, and has an intensity 100 times smaller than the first reflex. Consequently, the second and third reflex are usually only 3–4 cps above the background as shown in Fig. 11. The d values of the first three reflexes of the H_α phase are shown in Fig. 12.

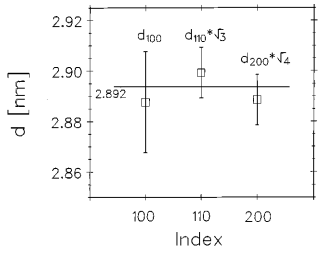

Fig. 12 d values of the first three XRD reflexes for $T = 363\,\mathrm{K}$ within the hexagonal phase of the KC_{12}/Gl system, $x_{KC_{12}} = 0.30$

Conclusions

As illustrated in Fig. 4b, in the binary system KC_{12}/Gl five phases appeared: the C phase, the L_α phase, the H_α phase, the G phase, and the S phase. The transition temperatures of the phase transitions were, in all cases, determined during sample heating, since it is well known that lyotropic liquid crystals can be easily undercooled. It is worth mentioning that the phase transition H_α ↔ S goes through a maximum.

The calorimetric and XRD measurements lead to the conclusion that the G phase appears below the H_α phase and not only below the L_α phase as previously assumed and illustrated in Fig. 4a. According to our additional measurements and results the phase diagram in Fig. 4a needs to be corrected as shown in Fig. 4b.

It is an essential result of our calorimetric and X-ray investigations that the texture observations, to establish a phase diagram, lead only to a rough knowledge of the phase regions in the phase diagrams. It is also necessary to apply calorimetry and XRD measurements. Especially it is difficult to identify the G phase only by texture observations using polarizing microscopy.

References

1. Dörfler HD, Senst A (1993) Colloid Polym Sci 271:173–189
2. Hieke A, Dörfler HD Colloid Polym Sci (in press)
3. Hieke A (1995) Thesis. TU Dresden
4. Freiberger Präzisionsmechanik GmbH (1991) Program manual APX 63/POWDER. Freiberg/Saxony, Germany
5. Chornik B, Sopizet R, Le Gressus C (1987) J Electron Spectrosc Relat Phenom 42:329–350
6. Morrison N (1969) Introduction to sequential smoothing and prediction. McGraw-Hill, New York
7. Hamming RW (1973) Numerical methods for scientists and engineers. International series in pure & applied mathematics McGraw-Hill, New York
8. Taylor FJ, Smith SL (1976) Digital signal processing in Fortran. Lexington. Lexington, Mass.
9. Blinchikoff HJ, Zverev AI (1976) Filtering in the time and frequency domains. Wiley, New York
10. Hamming RW (1977) Digital filters. Prentice-Hall signal processing series. Prentice-Hall, Englewood Cliffs, N.J.
11. Anderson BDO, Moore JB (1979) Optimal filtering. Prentice-Hall information and system sciences series. Prentice-Hall, Englewood Cliffs, N.J.
12. Chatfield C (1980) The analysis of time series: an introduction. Chapman and Hall, London
13. Wilmshurst TH (1985) Signal recovery from noise in electronic instrumentation. Adam Hilger, Bristol
14. Lim JS, Oppenheim AV (1988) Advanced topics in signal processing. Prentice-Hall signal processing series. Prentice-Hall, Englewood Cliffs, N.J.
15. Rorabaugh B (1993) Digital filter designer's handbook: featuring C routines. McGraw-Hill, New York
16. Koepcke RW, Patlach AM (1976) Smoother of discrete data. IBM invention disclosure bulletin. IBM, Armonk, N.Y. (June 1976) pp 292–293
17. Wooff C (1986) Comput Phys Commun 42:249
18. Fessler JA (1991) IEEE Trans Signal Process 39:852–859
19. Mierzwa B, Pielaszek J (1997) J Appl Crystallogr 30:544–546
20. Klug HP, Alexander LE (1974) X-ray diffraction procedures. Wiley, New York
21. Scout GH, Jensen LH (1989) X-ray structure determination. Wiley, New York
22. Smith H, Burge RE (1962) Acta Crystallogr 15:182–186
23. Commer DT, Waber JT (1965) Acta Crystallogr 18:104–109
24. Vand V (1948) Acta Crystallogr 1:109–115
25. Vand V (1948) Acta Crystallogr 1:290–291
26. McLachlan D, Lin HC (1973) Kristallogr 137:35–50
27. Werner PE: Trial-and error computer methods for the indexing of unknown powder patterns (1964) Z Kristallogr 120:375–387
28. Werner PE (1984) Documentation: trial and error program for indexing of unknown powder patterns (TREOR). Stockholm